*remote sensing*

MDPI

*Article*

# Can the Accuracy of Fine-Resolution Precipitation Products Be Assessed from the Surrounding Water Balance and Drought Chain (WBDC) in the Qinghai–Tibetan Plateau?

**Rui Li [1,*], Jiancheng Shi [2], Jinmei Pan [1,2], Nana Yan [1], Tianjie Zhao [1], Qingtao Zhang [3] and Yu Wang [4]**

[1] State Key Laboratory of Remote Sensing Science, Aerospace Information Research Institute, Chinese Academy of Sciences, Beijing 100101, China; panjm@aircas.ac.cn (J.P.); yannn@aircas.ac.cn (N.Y.); zhaotj@aircas.ac.cn (T.Z.)
[2] The National Space Science Center, Chinese Academy of Sciences, Beijing 100190, China; shijiancheng@nssc.ac.cn
[3] School of Civil Engineering, Sun Yat-sen University, Guangzhou 510275, China; zhangqt6@mail.sysu.edu.cn
[4] Hulunbeier Forestry and Grassland Development Center, Hailar 021000, China; yuwang202207@163.com
* Correspondence: lirui@radi.ac.cn

**Abstract:** The Qinghai–Tibetan Plateau (QTP), which has a unique and severe environment, suffers from the absence of rainfall gauges in western arid land. Using different precipitation products in this region would easily lead to contradictory results. To evaluate nine fine-resolution precipitation products in the QTP, we propose a "down to top" methodology, based on water balance and drought chain, by forecasting two accuracy assessment indices—multi-year precipitation bias and precipitation correlation. We assessed the biases of all products in the Jinsha–Yalong, Yellow, Heihe, Yangtze, Yarlung Zangbo catchments and interior drainage areas. And we assessed gauge-based correlation of precipitation products, based on the correlations between precipitation product-based effective drought index (EDI), Soil Moisture Active Passive (SMAP)-based soil moisture anomaly, and the moderate-resolution imaging spectroradiometer (MODIS)-based normalized difference vegetation index (NDVI) anomaly (R = 0.712, R = 0.36, and R = 0.785, respectively) for cross-sectional rainfall observations on the Tibetan Plateau in 2018. The results showed that ERA5-Land and IMERG merged precipitation dataset (EIMD) can efficiently close the water budget at the catchment scale. Moreover, the EIMD-based EDI exhibited the best performance in correlation with both the SMAP-based soil moisture anomaly and MODIS-based NDVI anomaly for the three main herbaceous species areas—Kobresia pygmaea meadow, Stipa purpurea steppe, and Carex moorcroftii steppe. Overall, we find that EIMD is the most accurate among the nine products. The annual average precipitation (2001–2018) was determined to be 568.16 mm in the QTP. Our assessment methodology has a remote sensing basis with low cost and can be used for other arid lands in the future.

**Keywords:** precipitation product; water balance; drought chain; effective drought index; soil moisture active passive; normalized difference vegetation index; herbaceous species



**Citation:** Li, R.; Shi, J.; Pan, J.; Yan, N.; Zhao, T.; Zhang, Q.; Wang, Y. Can the Accuracy of Fine-Resolution Precipitation Products Be Assessed from the Surrounding Water Balance and Drought Chain (WBDC) in the Qinghai–Tibetan Plateau? *Remote Sens.* **2024**, *16*, 79. https://doi.org/10.3390/rs16010079

Academic Editor: Gabriel Senay

Received: 9 November 2023
Revised: 16 December 2023
Accepted: 19 December 2023
Published: 24 December 2023



## 1. Introduction

The Qinghai–Tibetan Plateau (QTP) is usually called the "water tower of Asia" owing to its importance in the hydrological cycle. Many South and East Asian rivers originate from the QTP. In recent years, water balance issues in the QTP have attracted great attention. A recent study identified an imbalance in the Asian water tower caused by the accelerated transformation of ice and snow into liquid water [1]. Due to the harsh natural environment, such as continental glaciers [2] and the arid area in western QTP, there are only a few meteorological stations maintained by the China Meteorological Administration [3], which has caused uncertainties in determining the western part of the 400 mm isohyet [4].

Reanalysis products and remote sensing of precipitation are two significant supplements. Reanalysis methods merge background forecast models and data assimilation,

and their performance may depend on the quality of assimilated datasets [5], which are sparsely and non-representatively distributed in the QTP region. A variety of uncertainties of satellite-based precipitation products are associated with sensor accuracy, revisit time gaps, spatial resolution, relationships between remotely sensed signals and rainfall rates, and atmospheric effects [6]. Considering this context, scientific methods are required to assess the imperfect datasets in these remote areas with fewer gauges.

Precipitation is not a continuous variable and has strong spatial gradients. Rain gauges are the most common instruments to directly measure precipitation at the point scale [7]. However, rain gauges often suffer from low-density networks and frequent time-series gaps [8]. Previous precipitation evaluations show that station density is the most influential factor that affects grid data quality [9,10]. The density of existing observational stations on the QTP is much lower than for the rest of China. Most observation stations are in the central and eastern parts of the plateau, with few in the west [11]. A pertinent challenge is to identify other reliable methods to assess precipitation products. According to the principle of conservation of mass in closed systems, long-term water balance effectively partitions precipitation into runoff and evapotranspiration [12]. Unlike plot-based rain gauges, runoff at the catchment outlet represents the integrated response to all hydrological processes within the catchment [13]. The biases in precipitation climatologies are corrected based on worldwide streamflow observations [14].

As one of the most widespread and costly hydrological imbalance phenomena in the world [15], higher frequency and lower intensity of drought events occur in western QTP [16]. Reanalysis and remote sensing precipitation products-based drought indices were shown to be able to capture the occurrence and characteristics of drought events; however, they are influenced by various sources, the complex topography, and atmospheric processes [17,18]. The correlations of meteorological drought indices based on the Climate Hazards Group Infrared Precipitation with Stations (CHIRPS) in the QTP are better than those based on the Artificial Neural Networks-Climate Data Record (PERSIANN-CDR), the reason being that many spatial details of rain gauge observations are lost in the latter [19]. The Integrated Multi-Satellite Retrievals for Global Precipitation Measurement (IMERG) product has slightly better capability to capture meteorological drought than the Tropical Rainfall Measurement Mission (TRMM)-based Multi-satellite Precipitation Analysis (TMPA) product in Nepal and the southern QTP; gauge-based validation shows that this is because the IMERG product yields better performance in detecting precipitation and non-precipitation events than TMPA [20]. It seems that droughts, which are one example of an extreme event, can reflect the accuracy of precipitation products in the QTP. Droughts are usually classified as meteorological, agricultural, hydrological, or socioeconomic. Common to all types of drought is the fact that they originate from a deficiency of precipitation that results in water shortage [21]. Rainfed agricultural drought processes are validated by following the "precipitation–soil moisture–vegetative growth" drought chain diagram [22]. The development of space technology provides abundant remotely sensed data for vast areas with harsh weather conditions and complex topographies. Optical and microwave remote sensing is a useful tool for land surface soil moisture and vegetation monitoring in large areas. The Soil Moisture and Ocean Salinity (SMOS; European Space Agency, November 2009) and Soil Moisture Active Passive (SMAP; National Aeronautics and Space Administration, January 2015) missions are dedicated to the acquisition of global soil moisture information. The soil moisture products nominally released by SMOS and SMAP indicate average soil moisture at the top of the surface, which are conventionally compared with 5 cm in situ data [23]. The normalized difference vegetation index (NDVI) is the most used vegetation index, which is calculated based on remote sensing measurements of visible and near-infrared radiation. Stressed vegetation has positive but low values of NDVI [24]. The quality of the precipitation deficit can be evaluated by remote sensing-based component interactions during drought processes at specific species areas in the QTP.

In this paper, we attempt to evaluate nine fine-resolution (less than or close to 0.1 degree grid) precipitation products in the Qinghai–Tibetan Plateau based on the surrounding

drought chain and water balance rather than gauge observation. The specific objectives are to: (1) assess precipitation products against rain gauge observations in the QTP and predict gauge-based correlations based on drought chains; (2) assess the climatology characteristics of precipitation products based on water balance principles; (3) assess the correlation of precipitation products based on drought chains in the QTP; and (4) comprehensively evaluate the precipitation products.

## 2. Materials and Methods

### *2.1. "Down to Top" Surrounding Assessment Methodology*

Can the accuracy of precipitation products from the aspect of climatology and abnormal precipitation in arid areas be assessed using the internal relationships among internal constraints within the water cycle? Precipitation ($P$) can be regarded as the sum of precipitation climatology ($\overline{P}$) and precipitation abnormality ($\Delta P$). Precipitation climatology captures the central location or mean level of precipitation. Precipitation abnormality shows the departure of precipitation from normal levels.

$$P = \overline{P} + \Delta P \tag{1}$$

The key point of water balance or hydrologic balance is that the water amount on earth will never disappear and only moves within diverse geospheres during water cycle processes (Figure 1a). The great importance of the water balance equation, which posits that precipitation is equal to runoff plus evaporation and was first suggested by A. Penck in 1896 [12], is well known in hydrological sciences. The partition of precipitation into evapotranspiration and runoff at the land surface plays an important role in the Earth's hydrology and climate system [25,26]. Common precipitation abnormal phenomena are droughts and floods. The key point of the drought definition is the concept of a water deficit. Precipitation deficits are propagated over time through the surface runoff, soil moisture, streamflow, and groundwater components of the hydrologic cycle. Precipitation deficit is the dominant precipitation abnormality in arid areas of the QTP. Precipitation can be considered the first carrier of the drought signal [27]. According to the agricultural drought processing assessment framework [22], abnormal precipitation ($\Delta P$) at a specific site causes abnormal soil moisture ($\Delta SM$) and vegetation ($\Delta V$) through a condition anomaly. The positive correlation values among precipitation, soil moisture, and vegetation anomalies show the closeness of component relationships within the drought chain (Figure 1b). This suggests that abnormal precipitation is also likely to be assessed by their closeness within the drought chain.

### *2.2. The Framework for Precipitation Product Assessment*

We evaluate the fine-resolution precipitation products based on traditional gauge observations and our proposed surrounding assessment methodology (Figure 2). We evaluate the bias and correlation of two accuracy indices and employ pixel-based meteorological–soil moisture drought correlation and meteorological–vegetation drought to predict gauge-based assessment correlation. Surrounding evaluations include two aspects: we will first assess precipitation biases in sub-basins and large basins combined with multi-year average ET product values and watershed runoff observations. Based on microwave remote sensing soil moisture products and remote sensing vegetation products, we calculate meteorological–soil moisture drought correlation, meteorological–vegetation drought correlation and synthesis correlation to evaluate the correlations of precipitation products. Finally, we will comprehensively assess multiple precipitation products based on traditional gauge observations and our proposed assessment methodology.

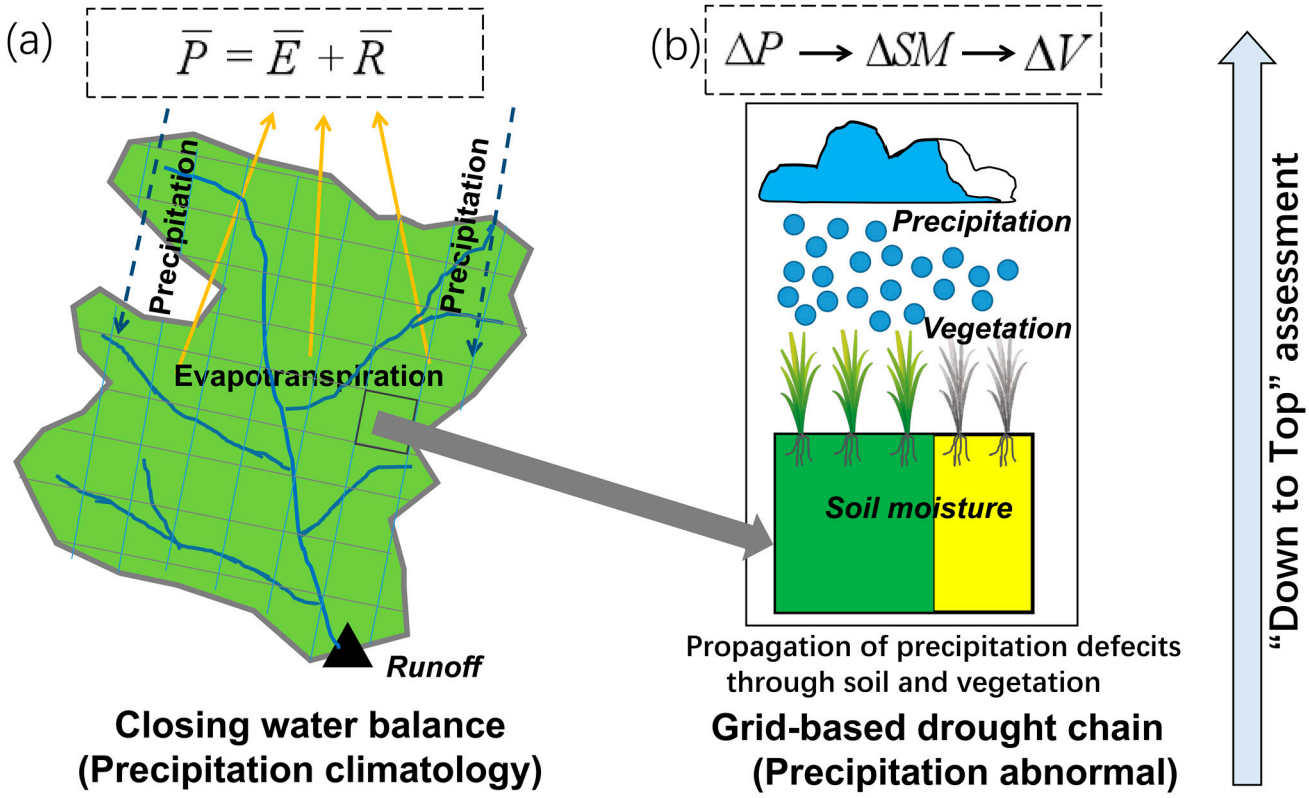


**Figure 1.** Precipitation assessment scheme based on the principles of water balance and the drought disaster chain.

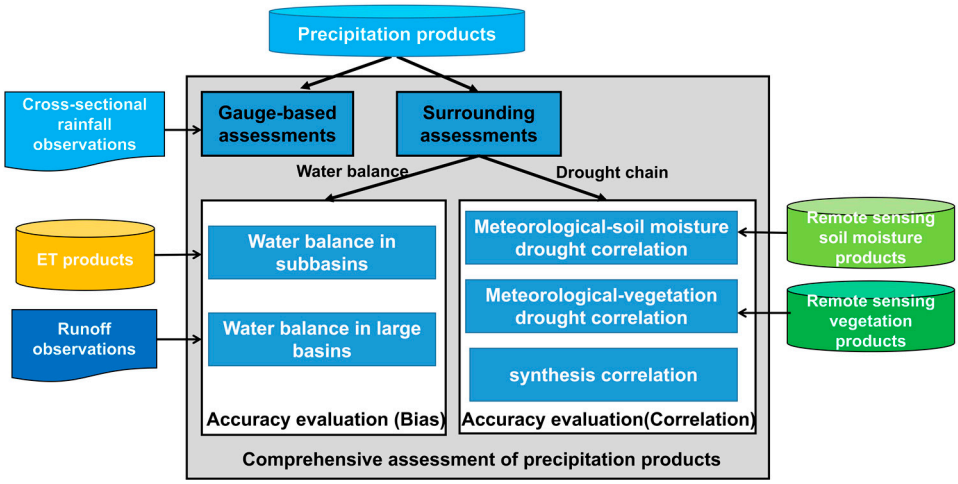


**Figure 2.** Flowchart of precipitation product assessment.

### *2.3. Study Area*

Five administrative provinces of China occupy the QTP (25–39°N, 73–105°E), with the average annual precipitation of this region decreasing from the southeast to the northwest as warm and humid air masses moving from the Indian Ocean are blocked by huge mountains. The QTP is the origin of several major rivers in Asia, including the Yarlung Zangbo River, Hei River, Yangtze River, Yellow River, and Lancang River (Figure 3a). A series of high mountains, including the Kunlun, Qilian, Tanggula, and Hengduan mountains, stretches along the plateau. We selected the Jinsha–Yalong river basin as our study area, including the Jinsha River (upper reaches of the panzhihua hydrological station) and the Yalong River, which is a major tributary river of the Yangtze River in Southwest China. A main feature of the rivers in this area is their large river fall (Figure 3b).

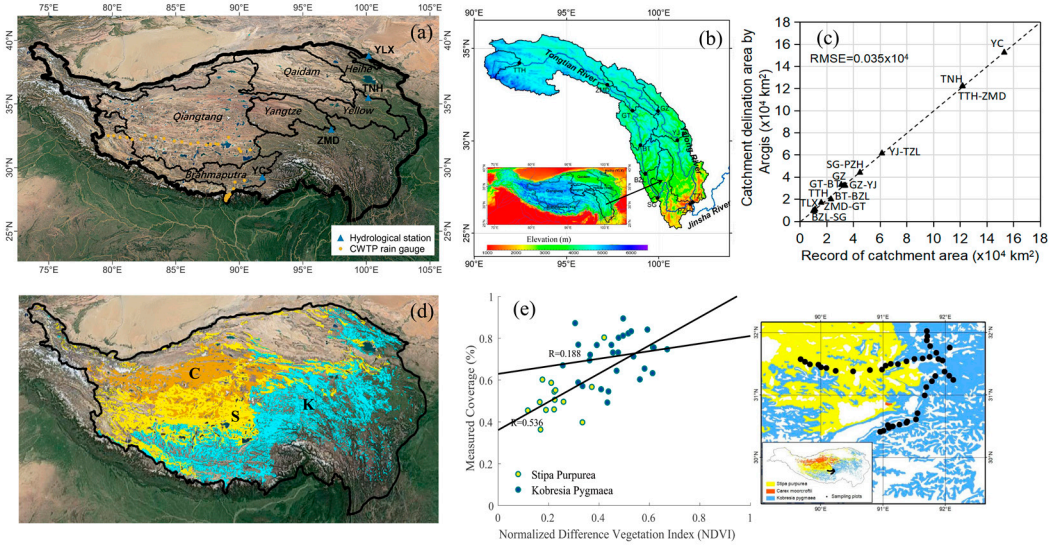


**Figure 3.** Study area: (**a**) locations of the six large catchment areas and CWTP rainfall gauges in the QTP, (**b**) location of drainage catchment in the Jinsha–Yalong basin, (**c**) fit of catchment delineation and catchment area records, (**d**) spatial pattern of Kobresia pygmaea meadow (K) (cyan color), Stipa purpurea steppe (S) (yellow color), and the Carex moorcroftii steppe (C) (red color), and (**e**) relationship between the measured vegetation coverage and MODIS vegetation NDVI in the herbaceous species areas.

The Vegetation Map of the People's Republic of China (1:1,000,000) is the scientific achievement of more than 200 scientists after more than 30 years of hard work. This atlas exhibits the whole picture of vegetation in China, including 55 vegetation types, 960 types of formations, and more than 2000 dominant plant species. For this study, three dominant grass species in the Tibet Plateau were selected—Kobresia pygmaea meadow, Stipa purpurea steppe, and Carex moorcroftii steppe, which occupy areas of $49.470 \times 10^4$ km$^2$, $39.245 \times 10^4$ km$^2$, and $19.832 \times 10^4$ km$^2$ within the Tibet Plateau, respectively (Figure 3d). The Kobresia pygmaea meadow, which represents the world's largest alpine ecosystem, is a common carpet-like sedge species found in the QTP. It has unisexual lateral spikes with slender yellow-green filiform leaves and normally grows in humid habitats above an elevation of 4000 m and below the local snow line [28]. The Stipa purpurea steppe is the dominant species of the Tibetan Plateau's alpine steppe and is endemic to the Tibetan Plateau and the Pamir Mountains of Central Asia, where it grows at elevations of 1900–5150 m a.s.l. [29,30]. Lastly, the Carex moorcroftii steppe is a widespread dominant sedge found in alpine steppes and meadows in the middle and northern parts of the Qiangtang Plateau.

### *2.4. High-Resolution Precipitation Product Materials*

#### 2.4.1. Gauge Rainfall Observation in the Central and Western Tibetan Plateau

Two observation transects running south–north and west–east across this region were used to obtain hourly rainfall data during the warm season (May–September). The south–north transect extends from Yadong Valley to Shuanghu County; the west–east transect extends from Shiquanhe to Naqu in the central TP [11]. We downloaded the hourly rain gauge data for the warm season (May–September) in the central and western Tibetan Plateau in 2018 from the National Tibetan Plateau Data Center DOI: 10.11888/Atmos.tpdc.272983 (accessed on 21 December 2023) and calculated total precipitation during the warm season for 19 stations along the south–north transect and for 20 stations along the west–east transect.

#### 2.4.2. Precipitation Products

We evaluated nine monthly-scale high-resolution precipitation products in the Qinghai–Tibetan Plateau according to our proposed method (Table 1). The time series of most datasets cover the period from 2001 to 2018. The datasets include: enhanced global dataset for the land component of the 5th generation of European ReAnalysis (ERA5-Land) [31], the Integrated Multi-satellitE Retrievals for GPM Final Precipitation L3 (GPM3 IMERGDF) 1 day 0.1 degree × 0.1 degree V06 [32], the China Meteorological Forcing Dataset (CMFD) [33], the Tibet Plateau Meteorological Forcing Dataset (TPMFD) [34], the PERSIANN-Cloud Classification System (PERSIANN-CCS) [35], monthly Multi-Source Weighted-Ensemble Precipitation (MSWEP) [36], the Climate Hazards Group InfraRed Precipitation (CHIRPS) with station data [37], and the bias correction CPC MORPHing technique product (CMORPH-ADL) [38]. We simply averaged monthly ERA5-Land precipitation and GPM IMERG precipitation as new datasets named ERA5-Land and IMERG Merged Dataset (EIMD), respectively, in this paper, as shown in Table 1.

**Table 1.** High-resolution precipitation products.

| Precipitation Product | Time Series | Spatial Resolution | Characteristics |
|---|---|---|---|
| ERA5-Land | 2001–2018 | 11.132 km | Integration of the ECMWF land surface model that is driven by downscaled meteorological forcing from ERA5 climate reanalysis. The monthly ERA5-Land products were from Copernicus Climate Data Store https://cds.climate.copernicus.eu/cdsapp#!/home (accessed on 21 December 2023) |
| GPM IMERG | 2001–2018 | 0.1 degree | Using both forward and backward morphing and including monthly gauge analyses, the final version of the dataset for 2001 to 2018 was downloaded from https://disc.gsfc.nasa.gov/datasets/GPM3IMERGHH06/summary?keywords=GPM (accessed on 21 December 2023) |
| CMFD | 2001–2018 | 0.1 degree | The dataset was created through a fusion of remote sensing products, reanalysis datasets, and in situ observation data at weather stations downloaded from DOI: 10.3972/westdc.002.2014.db (accessed on 21 December 2023) |
| CHIRPS | 2001–2018 | 0.1 degree | CHIRPS incorporates in-house climatology, CHPclim, 0.05-resolution satellite imagery, and in situ station data to create gridded rainfall time series for trend analysis and seasonal drought monitoring. Monthly dataset is available from https://data.chc.ucsb.edu/products/CHIRPS-2.0/global_monthly/netcdf (accessed on 21 December 2023) |
| CMORPH-ADL | 2001–2018 | 8 km | Bias correction is performed for the raw CMORPH through probability density function (PDF) matching against the CPC daily gauge analysis over land and through adjustment against the Global Precipitation Climatology Project (GPCP) pentad merged analysis of precipitation over the ocean. A 30 min dataset is available from the National Centers for Environmental Information https://www.ncei.noaa.gov/data/cmorph-high-resolution-global-precipitation-estimates/access/30min/8km (accessed on 21 December 2023) |
| MSWEP | 2001–2018 | 0.1 degree | The MSWEP product is unique in that it merges gauge, satellite, and reanalysis data. Monthly data are available from https://www.gloh2o.org/mswep/ (accessed on 21 December 2023) |
| TPMFD | 2001–2018 | 3 km | The ERA5 precipitation is corrected by high-resolution simulation at coarse spatial resolution and downscaled using a convolution neural network (CNN)-based model at the daily scale. |

**Table 1.** *Cont.*

| Precipitation Product | Time Series | Spatial Resolution | Characteristics |
|---|---|---|---|
| PERSIANN-CCS | 2003–2018 | 0.04 degree | PERSIANN-CCS system enables the categorization of cloud-patch features based on cloud height, areal extent, and variability of texture estimated from satellite imagery. Monthly datasets from 2003–2018 were from persiann.eng.uci.edu/CHRSdata/PERSIANN-CCS/mthly (accessed on 21 December 2023). |
| EIMD | 2001–2018 | 0.1 degree | Monthly average of ERA5-Land and IMERG, in this paper |

### *2.5. Other Datasets*

#### 2.5.1. Evapotranspiration

We downloaded five evapotranspiration datasets:

1. ERA5-land monthly total evaporation products [31] and ERA5 monthly total evaporation products were downloaded from Copernicus Climate Data Store https://cds.climate.copernicus.eu/cdsapp#!/home (accessed on 21 December 2023)
2. ETMonitor Global actual evapotranspiration dataset 1-km resolution [39] from 2001–2018 was downloaded from https://www.tpdc.ac.cn/. DOI:10.11888/Hydro.tpdc.270298.CSTR:18406.11.Hydro.tpdc.270298 (accessed on 21 December 2023)
3. Monthly mean evapotranspiration dataset for the Tibet Plateau (2001–2018) [40] was downloaded from https://www.tpdc.ac.cn/. DOI:10.11888/Hydro.tpdc.270995.CSTR:18406.11.Hydro.tpdc.270995 (accessed on 21 December 2023)
4. GLDAS Noah Land Surface Model L4 0.25 × 0.25-degree V2.1 evapotranspiration dataset [41], which forces the combination of model and observation data, was downloaded from the Goddard Earth Sciences Data and Information Services Center https://disc.gsfc.nasa.gov/datasets/GLDASNOAH025M2.1/summary?keywords=gldas (accessed on 21 December 2023)

#### 2.5.2. Runoff Dataset

We collected and calculated a multi-year average runoff dataset for the Zhimenda station on the Tongtian River (2001–2012) [42]. Tangnaihai station data on the Yellow River (2001–2018) were from the Yellow River Conservancy Commission of the Ministry of Water Resources. Yangcun station (2001–2014) and Yingluoxia station (2001–2015) data on the Yarlung Zangbo River were from a local survey bureau of hydrology (Figure 3a). As sub-basins of the Jinsha–Yalong watershed, 4-year average runoff data for seven stations in the Jinsha River basin—Tuo-tuohe, Zhimenda, Batang, Gangtuo, Benzilan, Shigu, and Panzhihua—and three stations in the Yalong River basin—Ganzi, Yajiang, and Tongzilin—in 2011, 2012, 2017, and 2018 were collected and calculated from the Annual Hydrological Report of the P.R.C. We delineated the catchments of all stations based on HydroSHEDS https://www.hydrosheds.org (accessed on 21 December 2023), which is derived from elevation data of the Shuttle Radar Topography Mission (SRTM) at 3 arc-second resolution. Comparisons of areas delineated by ARCGIS ver. 10.8 software (Esri Inc., Redlands, CA, USA) and station drainage areas show that the RMSEs of all catchments is $0.035 \times 10^4$ km$^2$ (Figure 3c).

#### 2.5.3. Microwave Remote Sensing-Based Soil Moisture Dataset

We extracted daily SMAP-enhanced L3 radiometer soil moisture (SPL3SMP_E.005) data from 2015 to 2018 for the QTP domain using an application for extracting and exploring analysis-ready samples (AppEEARS) https://appeears.earthdatacloud.nasa.gov/ (accessed on 21 December 2023), which offers a simple and efficient way to access and transform geospatial data from a variety of federal data archives.

#### 2.5.4. Vegetation Remote Sensing and Survey Dataset

The Global MODIS NDVI dataset (MOD13A3) data are provided as a 1 km gridded Level 3 product every month. Drawing on this, we extracted the NDVI dataset from 2015 to 2019 for the Tibet Plateau domain using AppEEARS. We also employed the Qinghai–Tibetan plateau vegetation survey data (2019) provided by the National Tibetan Plateau Data Center http://data.tpdc.ac.cn. DOI: 10.11888/Terre.tpdc.272863.CSTR: 18406.11.Terre.tpdc.272863. (accessed on 21 December 2023), which includes the vegetation coverage dataset extracted using the belt transect method for 44 sampling plots in Northern Tibet. The dataset was collected from July to August 2019. For each plot, there were 10 sampling sites with measurements of 50 cm × 50 cm. We calculated the average coverage of the sampling sites for each plot. Among the 42 vegetation measurement plots evaluated during the 2019 summer field survey, 14 plots were located in the Stipa purpurea-dominated area, and 28 were located in the Kobresia pygmaea-dominated area (Figure 3e). The correlation between the measured coverage and the MODIS NDVI served to demonstrate the characteristics of the different species. With an increase in the NDVI, the coverage of Stipa purpurea showed an increasing linear trend (R = 0.536). By contrast, a slight increase in the coverage of Kobresia pygmaea was observed with an increase in the NDVI (R = 0.188).

### *2.6. Drought Indices*

The drought chain was evaluated based on the precipitation-based index, the evapotranspiration-based index, the soil moisture-based index, and the MODIS vegetation-based index. The correlation coefficient ($R$) was employed to evaluate the interactions during the drought chain "precipitation–soil moisture–vegetation" procedure.

#### 2.6.1. Precipitation-Based Index

The effective drought index (EDI) [43] is appropriate for the operational monitoring of meteorological and agricultural drought situations, with a single input required for calculations. The EDI program (FORTRAN 90) was employed to caculate monthly EDI. The calculation procedure is as follows:

5. Calculate the monthly $EP$ (Equation (2)).

$$EP = \sum_{n=1}^{i} \left[ \left( \sum_{m=1}^{n} P_m \right) / n \right] \tag{2}$$

where $i$ is the period over which the sum of the precipitation is calculated, which is generally the most common precipitation cycle. Furthermore, $P_m$ denotes the precipitation that occurred m days ago. Thus, $EP$ denotes the usable precipitation accumulated for the entire year.

6. Calculate the mean $EP$ ($MEP$) for each month.
7. Calculate the difference between the $EP$ and $MEP$, which is $DEP$ (Equation (3)).
8. When the $DEP$ is represented by a negative number, it indicates conditions drier than the average. If this dry period continues, add the days of prolonged dryness to the existing period and recalculate the $EP$ for that specific period.
9. Calculate the $MEP$ and $DEP$ again.
10. Divide the monthly $DEP$ using the standard deviation ($SD$) of the $DEP$ over the past years (Equation (4)).

For the time series of precipitation products, this paper defines the period from 2002–2018 as the reference climate years. Finally, we calculated the monthly EDI based on the nine precipitation datasets.

$$DEP = EP - MEP \tag{3}$$

$$EDI = DEP/SD(DEP) \tag{4}$$

2.6.2. Soil Moisture-Based Index

We calculated the soil moisture anomaly index ($SMAI$) based on the SMAP soil moisture and average soil moisture data (Equation (5)), with $i$ and $j$ representing the specific year and month, respectively, pertaining to the data:

$$SMAI_{i,j} = \frac{SM_{i,j} - SM_{i,ave}}{SM_{i,ave}} \tag{5}$$

2.6.3. MODIS Vegetation-Based Index

We calculated the NDVI anomaly ($NDVIA$) based on the MODIS monthly NDVI data (Equation (6)), with $i$ and $j$ representing the specific year and month pertaining to the data:

$$NDVIA_{i,j} = \frac{NDVI_{i,j} - NDVI_{i,ave}}{NDVI_{i,ave}} \tag{6}$$

*2.7. Statistical Methodology*

2.7.1. Assessment Indices

We used Pearson's correlation coefficient ($R$), which indicates the strength of the linear relationship between the values of the monthly rain gauge observations ($O_m$) and precipitation product values ($P_m$), ranging from $-1$ for an inverse linear relationship to 1 for a perfect linear relationship (Equation (7)). The bias, which shows systematic deviations of precipitation products' multi-year average values (P) in relation to the not estimated values ($\hat{P}$), is simultaneously a measure of deviation because it does coincide with the real value and is systematic because it occurs consistently on average (Equation (8)).

$$R(P_m, O_m) = \frac{\mathrm{Cov}(P_m, O_m)}{\sigma(P_m, O_m)} \tag{7}$$

$$Bias = \frac{1}{N}\sum_{i=1}^{N}(P - \widehat{P}) \tag{8}$$

2.7.2. Predictors for Correlation Estimations

We employed three predictors, meteorological–soil moisture drought $PR1$ (Equation (9)), meteorological–vegetation drought $PR2$ (Equation (10)), and synthesis $PR3$ (Equation (11)), to estimate gauge-based assessment correlation: $PR1$—$SMAI$–$EDI$ correlation, $PR2$—$NDVIA$–$EDI$ correlation, and $PR3$—arithmetic mean of $SMAI$–$EDI$ correlation and $NDVIA$–$EDI$ correlation in specific pixels. As cross-sectional rainfall observation was used for TPMFD product validation (private conversation), eight products except TPMFD were employed to predict gauge-based assessment correlation.

$$PR1(SMAI, EDI) = \frac{Cov(SMAI_{i,j}, EDI_{i,j})}{\sigma(SMAI_{i,j}, EDI_{i,j})} \tag{9}$$

$$PR2(NDVIA, EDI) = \frac{Cov(NDVIA_{i,j}, EDI_{i,j})}{\sigma(NDVIA_{i,j}, EDI_{i,j})} \tag{10}$$

$$PR3(SMAI, EDI) = \frac{R(SMAI_{i,j}, EDI_{i,j}) + R(NDVIA_{i,j}, EDI_{i,j})}{2} \tag{11}$$

where $PR1$, $PR2$, $PR3$ is the correlation predictor, and $i$ and $j$ are the pixel column and line serial number, respectively.

## 3. Results

### *3.1. Validation Based on Rain Gauge Observations*

The rainfall observations from May to September 2018 showed that, compared with other products, TPMFD and EIMD precipitation products had the maximum R. CMORPH and PERSIANN-CCS had the minimum R. From the aspect of RMSE, except MSWEP, all other products overestimated the observations. TPMFD had the minimum RMSE of 30.04 mm, while ERA5-Land had the maximum RMSE of 234.7 mm (Figure 4). Compared with south–north cross-sectional rainfall observations of 19 gauges, the ERA5-Land, IMERG, and CMFD had the largest precipitation bias for the gauges between 27°N and 28°N and PERSIANN-CCS had increasing bias with increase in latitude (Figure 5a). Compared with the west–east cross-sectional rainfall observations of 20 gauges, CMORPH had larger precipitation bias for the gauges between 84° and 92°E. In contrast, the MSWEP had minus bias for the gauges between 84° and 87°E. The PERSIANN-CCS had increasing bias with increase in longitude (Figure 5b). Compared to the precipitation observations from overall gauges, all the nine products overestimated total precipitation from May to September 2018. ERA5-Land, PERSIANN-CCS, and EIMD had the largest bias, while CMFD, MSWEP, and TPMFD had the smallest bias (Figure 5c). We predicted their gauge-based correlation ($r$) by using the "precipitation–soil moisture–vegetation" drought chain method. The results showed that we estimated the $R$ of eight precipitation products based on the $PR1$ correlation between EDI and SMAP soil moisture with a fitness correlation of 0.712. Further, we estimated the $R$ of eight precipitation products based on the $PR2$ correlation between EDI and NDVI with a fitness correlation of 0.36. When we calculated the average $R$ of both the SMAP-based correlation and the NDVI-based $PR3$ correlation, the fitness correlation was 0.785 (Figure 6).

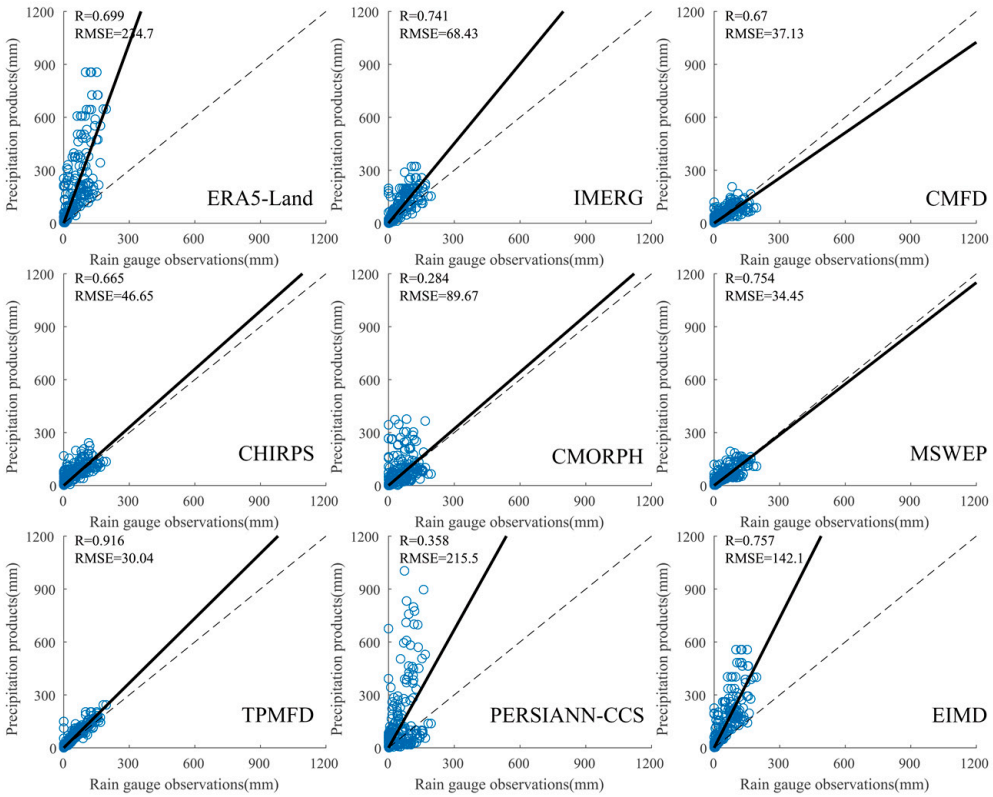


**Figure 4.** Monthly precipitation products validated by all cross-sectional rainfall observations on the Tibetan Plateau in the warm season in 2018.

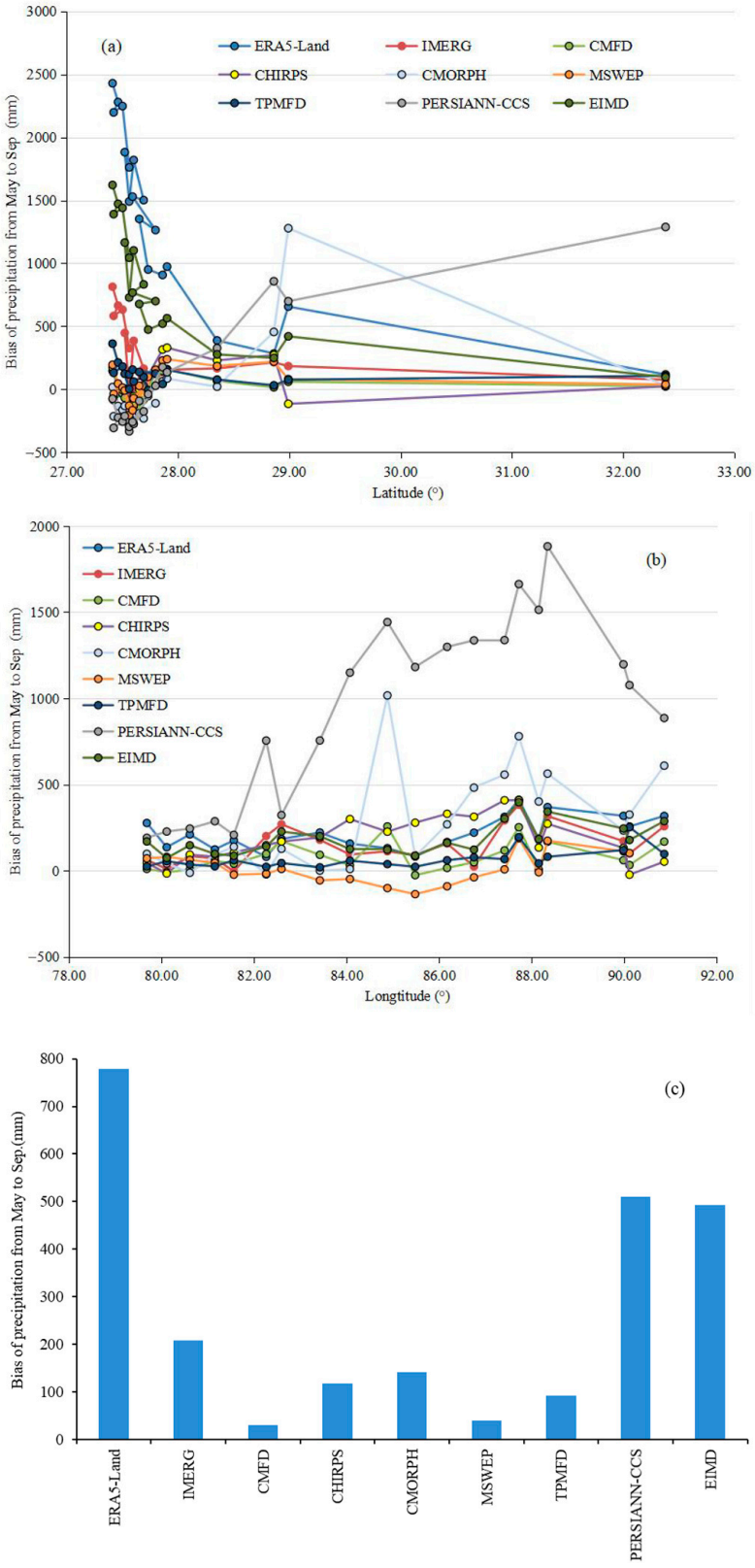


**Figure 5.** Bias of precipitation products vis a vis the Tibetan Plateau in the warm season in 2018 from May to September compared to (**a**) west–east cross-sectional rainfall observations of 19 gauges, (**b**) south–north cross-sectional rainfall observations of 20 gauges, and (**c**) all cross-sectional rainfall observations.

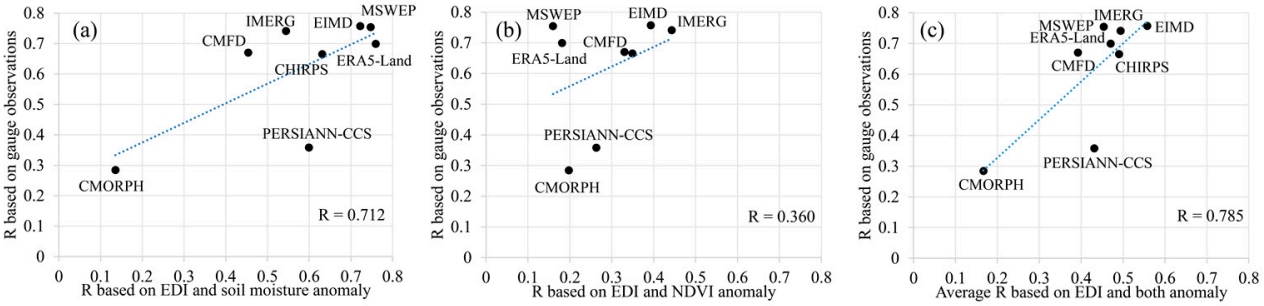


**Figure 6.** Predictions of gauge-based correlation (R) using the correlation of eight precipitation products based on EDI and (**a**) SMAP soil moisture anomaly, (**b**) NDVI anomaly, and (**c**) both anomalies.

### *3.2. Evaluation of Precipitation Climatology in QTP Based on Water Balance Principles*

Multi-product comparisons between four-year (2011, 2012, 2017, and 2018) average annual precipitation products and annual precipitation estimates based on runoff and five ET products were conducted for 10 sub-basins of the Jinsha–Yalong basin. Upon adding all five ET products to runoff, ERA5-Land ET, ERA5 ET, ETMonitor, and GLDAS ET showed high RMSE and overestimated precipitation values. The RMSE obtained by adding MET to the ERA5-Land precipitation provided a precipitation value of 80.86 mm. By contrast, adding the values of all five ET products to runoff led to an underestimation of precipitation by IMERG, CMFD, CHIRPS, CMORPH, and MSWEP. Upon adding all five ET products to the runoff, PERSIANN-CCS precipitation exhibited the worst fit.

Meanwhile, upon adding all five ET products to runoff, ERA5 and ERA5-Land ET exhibited better fit to TPMFD and EIMD precipitation values. Especially upon adding all the ET products to runoff, ERA5 and ERA5-Land ET exhibited the best fit to EIMD precipitation values with the highest Rs of 0.924 and 0.929, respectively, and the lowest RMSEs of 56.79 and 49.8 mm, respectively (Figure 7).

Multi-product comparisons of average annual precipitation products and annual precipitation estimates based on runoff and ERA5-Land in the Jinsha–Yalong, Yellow, Heihe, Yarlung Zangbo catchments, and the Qiangtang and Qaidam interior drainage areas of central and eastern Qinghai–Tibetan Plateau showed that the multi-year ERA5-Land and PERSIANN-CCS precipitations overestimated drainage runoff and ERA5-Land evapotranspiration. Meanwhile, multi-year IMERG precipitation underestimated drainage runoff and ERA5-Land ET, as did multi-year CMFD, CHIRPS, CMORPH, MSWEP, and TPMFD precipitation. By contrast, multi-year EIMD and TPMFD precipitation achieved improved agreement with regard to runoff and ERA5-Land ET. EIMD yielded the second largest R and the second smallest RMSE for all large basins. By contrast, PERSIANN-CCS yielded the smallest R and highest RMSE for all large basins (Figure 8).

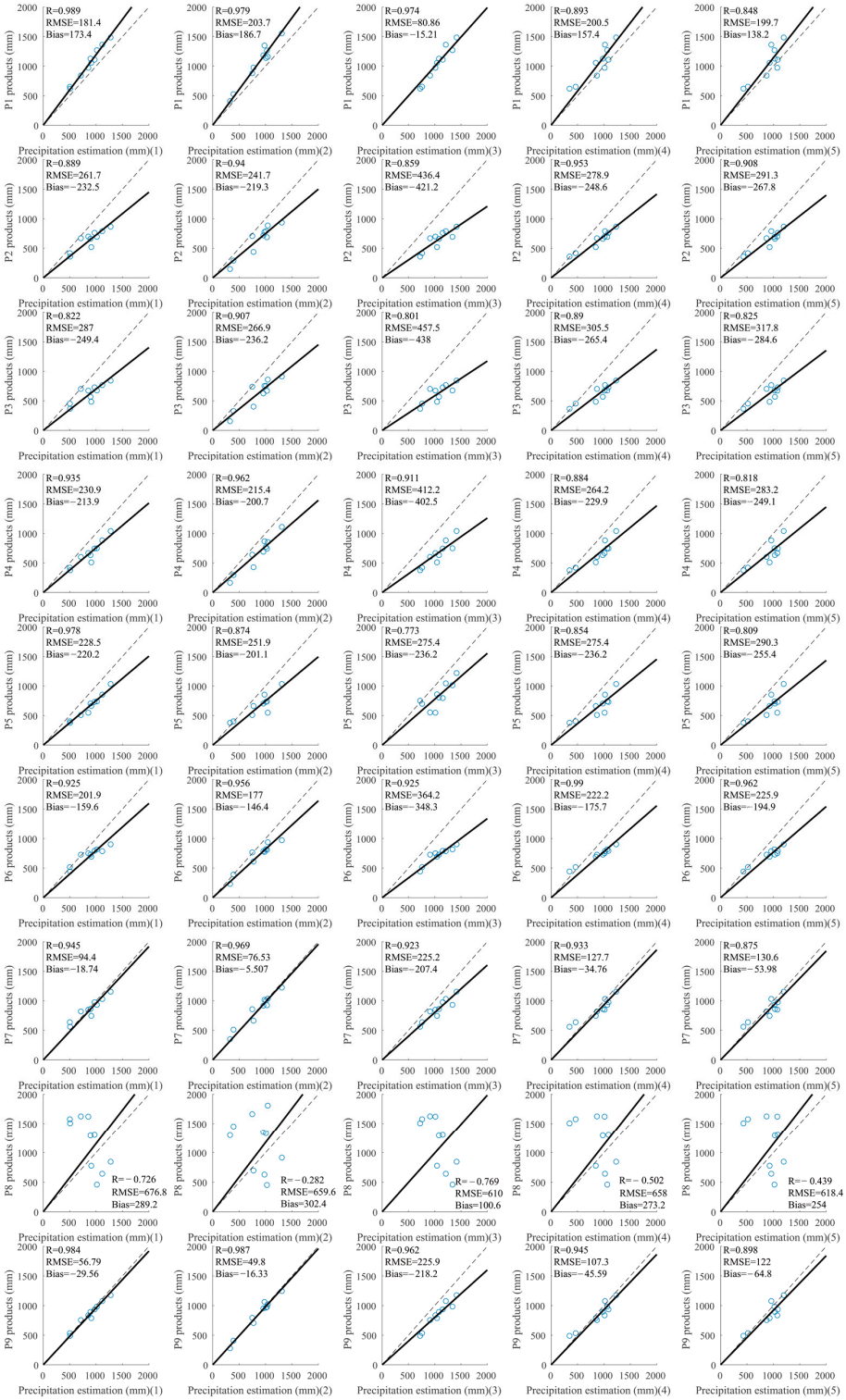


**Figure 7.** Evaluation of nine precipitation products based on 4-year average annual runoff and ET products in 10 sub-basins of the Jinsha–Yalong: P1 = ERA5-Land, P2 = IMERG, P3 = CMFD, P4 = CHIRPS, P5 = CMORPH, P6 = MSWEP, P7 = TPMFD, P8 = PERSIANN-CCS, P9 = EIMD, (1) = ERA5-Land ET, (2) = ERA5 ET, (3) = ETa-TP-SEBS ET, (4) = GLDAS ET, (5) = ETMonitor ET.

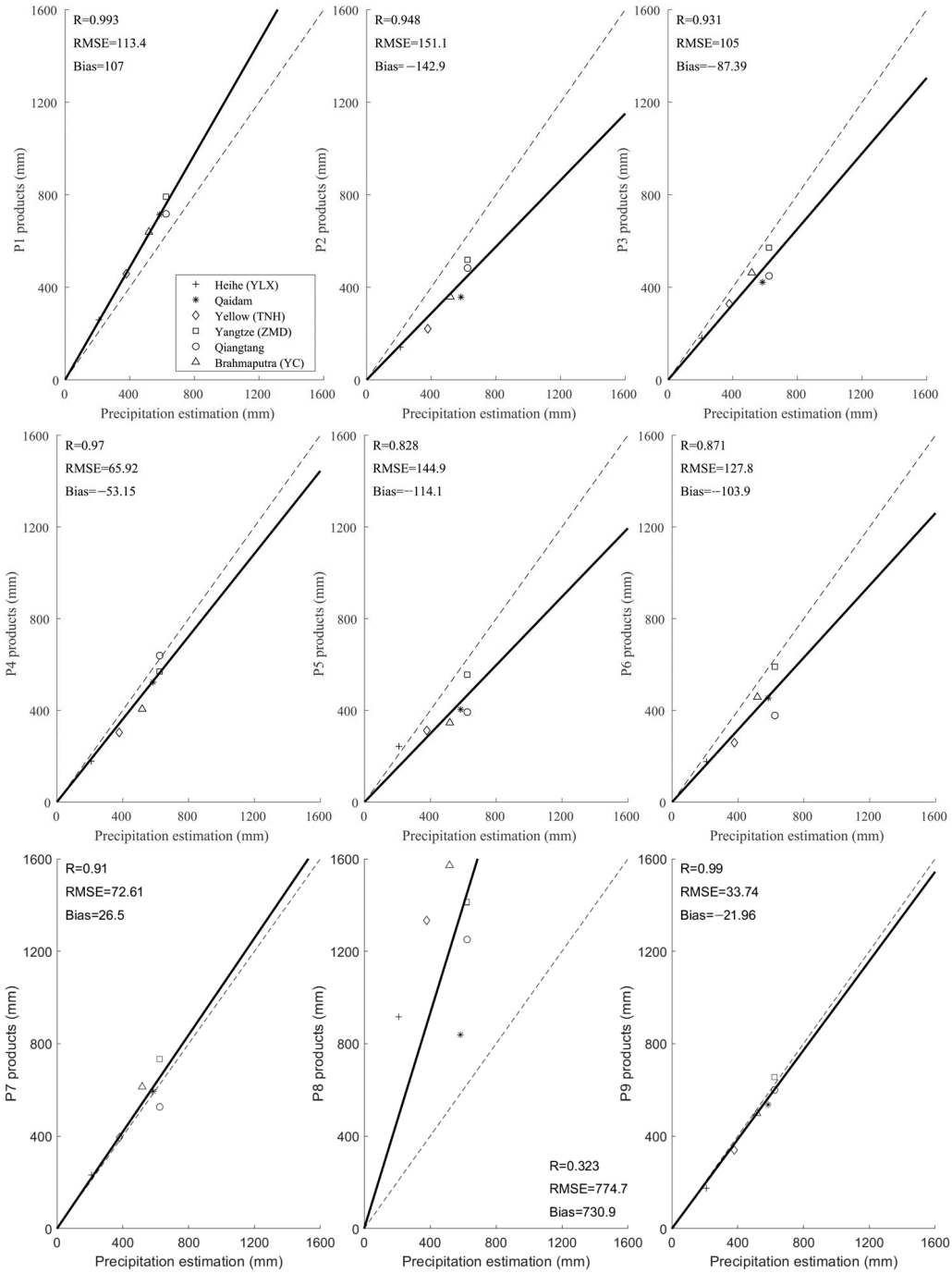


**Figure 8.** Evaluation of nine precipitation products based on 4-year average annual runoff and ERA5-Land ET in HeiheQai dam, Yellow River, Yangtze, Qiangtang, and Brahmaputra basins: P1 = ERA5-Land, P2 = IMERG, P3 = CMFD, P4 = CHIRPS, P5 = CMORPH, P6 = MSWEP, P7 = TPMFD, P8 = PERSIANN-CCS, P9 = EIMD.

### *3.3. Evaluation of Precipitation Product Correlation for the QTP Based on Drought Chains*

According to the cumulative percentage of correlation between SMAP and the effective drought index, the average correlations of indices for different products followed the order EIMD > ERA5-Land > MSWEP > IMERG > CHIRPS > TPMFD > CMFD > CMORPH > PERSIANN-CCS (Figure 9). We compared nine precipitation products in the three vegetation areas from 2015 to 2018 based on SMAP soil moisture, MODIS NDVI, and both. The average R of EIMD exhibited the highest values in all three vegetation areas. These were 0.597 in the Carex moorcroftii steppe, 0.535 in the Stipa purpurea steppe, and

0.549 in the Kobresia pygmaea meadow. In the Kobresia pygmaea meadow, the average R of IMERG (0.537) was higher than that of ERA5-land (0.397). By contrast, in the Stipa purpurea steppe and the Carex moorcroftii steppe, the average Rs of ERA5-Land (0.524, 0.582) were higher than those of IMERG (0.446, 0.506). For the entire QTP region, the results showed that the average Rs of the different products followed the order EIMD (0.563) > MSWEP (0.512) > IMERG (0.509) > CHIRPS (0.500) > ERA5-Land (0.486) > TPMFD (0.427) > CMFD (0.365) > CMORPH (0.343) > PERSIANN-CCS (0.076). EIMD exhibited the highest R, and PERSIANN-CCS exhibited the lowest R (Figure 10).

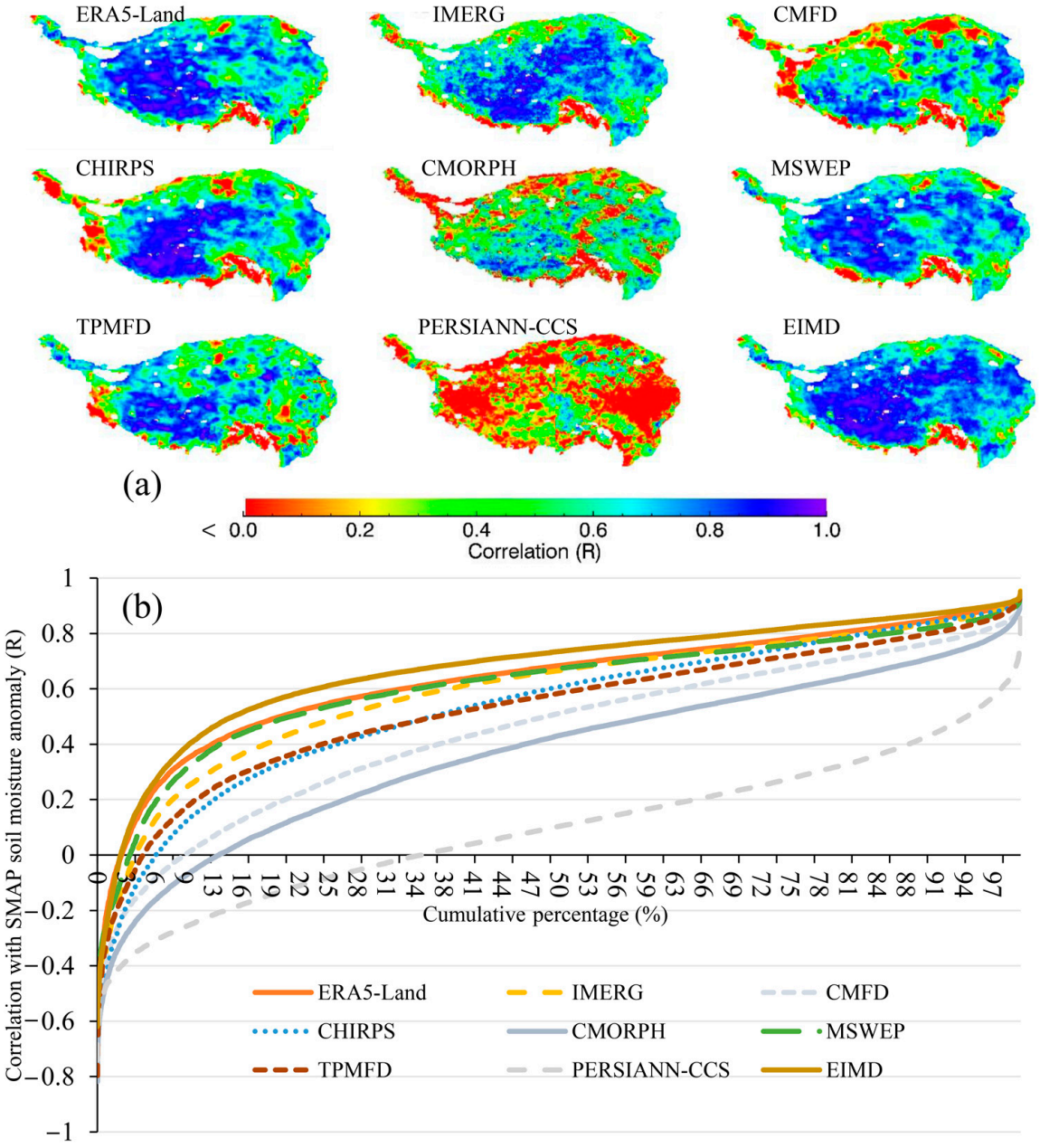


**Figure 9.** Correlations between monthly SMAP soil moisture and effective drought index (EDI) from 2015 to 2018: (**a**) correlation maps and (**b**) cumulative percentages.

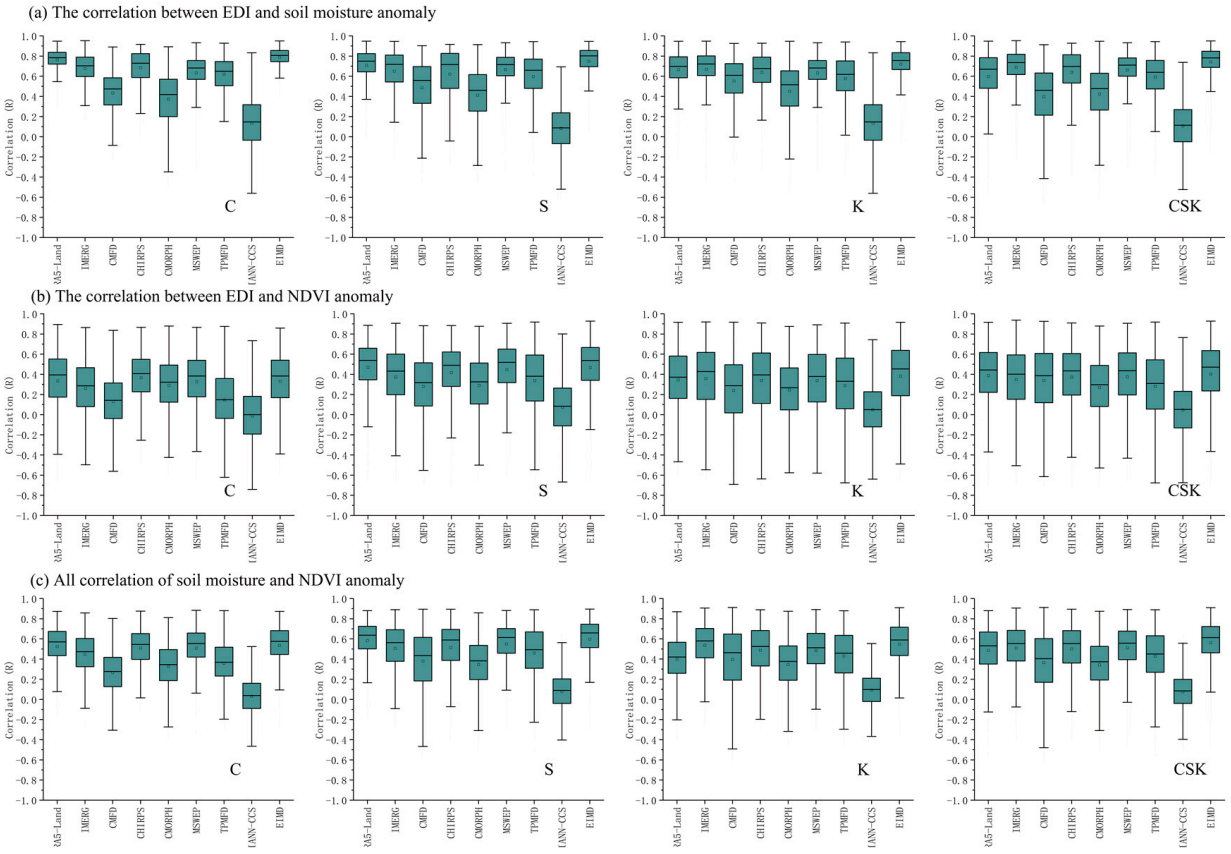


**Figure 10.** Correlations between monthly NDVI and effective drought index (EDI) from 2001 to 2018 in the Kobresia pygmaea meadow (K), the Stipa purpurea steppe (S), the Carex moorcroftii steppe (C), and in all three areas (CSK).

### *3.4. Comprehensive Evaluation of Precipitation Products*

We summarized diverse assessments based on gauges, runoff observations, and drought chains (Table 2). The results showed that CMFD, MSWEP, and TPMFD were the top three precipitation products during the warm season based on bias evaluation against gauge observations. TPMFD, EIMD, and MSWEP were the top three precipitation products during the warm season based on correlation evaluation against gauge observations. The ranking of PERSIANN-CCS was 8, based on both bias and correlation evaluations against gauge observations. The ranking of EIMD was 7 based on bias evaluation of gauges from May to September. The ranking of EIMD was 2 based on correlation evaluation against gauges and drought chain in the Stipa purpurea steppe. EIMD ranked as the top based on watershed runoff and drought chain in the Carex moorcroftii steppe, the Kobresia pygmaea meadow, and all three vegetation areas. EIMD was evaluated as the best precipitation product for the QTP. By contrast, PERSIANN-CCS ranked bottom in all three vegetation areas and watershed runoff. Further, the ranking of PERSIANN-CCS was 8 based on bias and correlation evaluation against gauges from May to September. PERSIANN-CCS can be regarded as the worst precipitation product with regard to the QTP. Thus, we determined that the annual average precipitation (2001–2018) in the QTP was 568.16 mm based on EIMD.

**Table 2.** Summary of precipitation assessments based on gauges, runoff observations, and drought chain.

| From High to Low Quality | Bias Based on Gauges (May to Sep.) | Correlation Based on Gauges (May to Sep.) | Bias Based on Watershed Runoff | Correlation Based on Drought Chain | | | |
|---|---|---|---|---|---|---|---|
| | | | | Carex Moorcroftii Steppe (C) | Stipa Purpurea Steppe (S) | Kobresia Pygmaea Meadow (K) | All Three Varieties (CSK) |
| 1 | CMFD | TPMFD | EIMD | EIMD | ERA5-Land | EIMD | EIMD |
| 2 | MSWEP | EIMD | TPMFD | ERA5-Land | EIMD | IMERG | MSWEP |
| 3 | TPMFD | MSWEP | CHIRPS | MSWEP | MSWEP | CHIRPS | IMERG |
| 4 | CHIRPS | IMERG | CMFD | CHIRPS | CHIRPS | MSWEP | CHIRPS |
| 5 | CMORPH | ERA5-Land | MSWEP | IMERG | IMERG | TPMFD | ERA5-Land |
| 6 | IMERG | CMFD | ERA5-Land | TPMFD | TPMFD | ERA5-Land | TPMFD |
| 7 | EIMD | CHIRPS | CMORPH | CMORPH | CMFD | CMFD | CMFD |
| 8 | PERSIANN-CCS | PERSIANN-CCS | IMERG | CMFD | CMORPH | CMORPH | CMORPH |
| 9 | ERA5-Land | CMORPH | PERSIANN-CCS | PERSIANN-CCS | PERSIANN-CCS | PERSIANN-CCS | PERSIANN-CCS |

## 4. Discussion

### *4.1. The Water Balance Method for Estimating Precipitation Accuracy*

Some research shows that water is imbalanced on the QTP [44]. But our results showed that, compared with the five ET products, there were greater uncertainties associated with the nine precipitation products with regard to the QTP (Figures 7 and 8). The influence of human water use on runoff is limited in the QTP [45]. EIMD and ERA5-Land ET could efficiently close the water balance in the Jinsha–Yalong, Yellow, Heihe, Yangtze, Yarlung Zangbo catchments and interior drainage areas. Therefore, we propose that the water still maintains balance in the QTP. Precipitation is partitioned into terrestrial water balance components, such as fluxes (evaporation, transpiration, runoff) and, what is more, changes in storage (soil moisture, groundwater) [46]. A recent study showed that there is a seasonal recharge–storage–runoff process combined with monthly Gravity Recovery and Climate Experiment (GRACE) dataset [47]. The seasonal bias of precipitation is expected to be evaluated using the water balance method. Bias seems more appropriate than correlation coefficient to select the best rainfall product for hydrological modelling [48]. Our proposed evaluation methodology of precipitation bias based on water balance could help to select precipitation product before applying hydrological simulations in future.

### *4.2. The Drought Chain Method for Estimating Precipitation Accuracy*

There are significant temporal effects of drought on vegetation in grassland areas of the QTP during the growing season, which reach their peak in July and August. Compared to the east monsoon region, most of the western regions have higher-frequency and lower-intensity drought events [16]. The drought chain phenomenon commonly occurs in western regions of the QTP where precipitation observations are lacking. Compared with SMOS-IC, FY3B, JAXA, and LPRM soil moisture products, the uncertainty of SMAP is lowest over the entire QTP [49]. The accuracy of reanalysis and remote sensing precipitation products is affected by extreme precipitation events. For instance, the best precipitation estimate from IMERG was for moderate rainfall levels rather than for light and extreme rainfalls [50,51]. There are similar spatial patterns in the correlations between AMSR-E soil moisture and NDVI and between EDI and NDVI in northern China [52]. This study further validated that there is a close relationship between EDI and SMAP soil moisture in the QTP (Figure 9). Precipitation frequency contributed more than total precipitation to peak vegetation growth in the Tibetan Plateau, especially in arid areas [53]. Our drought chain method reveals monthly precipitation changes. Diverse mechanisms of arid and humid biomes determine the sensitivity of biomes to drought [54]. Unlike herbaceous plants, during drought events, the deep root systems of woody plants can help them withstand drought stress [55]. We considered the Kobresia pygmaea meadow, the Stipa purpurea steppe, and the Carex moorcroftii steppe as three herbaceous species in the QTP. Our results demonstrate the importance of selecting representative vegetation when using our evaluation method in other regions. Moreover, drought propagation is closely related to the water cycle. Satellites enable more comprehensive estimation of multiple aspects of the water cycle, such as

lake level and volume changes [56,57]. More factors in the water environment should be considered in drought chain processes.

### *4.3. Comprehensive Evaluation of Precipitation Products*

There are mismatches between station-based precipitation observations at the point scale and pixel-based precipitation products. Our water balance and drought chain methodology has advantages at the grid or watershed scale. The largest precipitation biases relative to the south–north cross-sectional rainfall observations of 19 gauges occurred between 27°N and 28°N (Figure 5) due to greater overestimation/underestimation in regions with higher precipitation rates [58]. Previous evaluation of precipitation products in the Qinghai–Tibetan Plateau based on 83 China Meteorological Administration rainfall gauges showed that MSWEP and CHIRPS can represent the spatial patterns of climatological precipitation. PERSIANN_CCS has poor performance [59]. In the periphery of Tibetan Plateau, precipitation assessment showed that CHIRPS outperforms PERSIANN-CCS in all seasons in northwest Pakistan [60]. CHIRPS and MSWEP are more skillful than CMORPH and real-time PERSIANN-CCS-Adj. across complex topographical and climatic gradients [61]. MSWEP shows better correlation than CHIRPS in the highlands of Indo-Pak [62]. These findings support the interpretation of our evaluation results. Our study shows that, compared to cross-sectional rainfall observations in the Tibetan Plateau, most precipitation products overestimate precipitation (Figures 4 and 5). This is due to wetting losses, trace precipitation, wind undercatch and evaporation losses of gauge observations [63]. Runoff observations and drought chains are a more reliable basis. CMFD and TPMFD merge daily ground observations from the China Meteorological Administration [33,34]. Cross-sectional rainfall observations were used for TPMFD validation. These reanalysis products performed well against gauge observations. A previous study showed that ERA5-Land presents severe overestimations of precipitation amount. IMERG products outperform ERA5-Land in estimating precipitation amount in the Tibet Plateau. However, the simulation performance of ERA5-Land is comparable to IMERG by hydrological model in the Yellow River [64]. Our study shows that IMERG is better than ERA5-Land in three herbaceous species areas (Table 2), which is comparable to the results of previous studies. The comparison of GPM IMERG with nine satellite and reanalysis products in China reveals that, although the IMERG product outperforms most datasets, IMERG underestimates snowfall compared with gauge and reanalysis data [65]. Our results show that the simple average method for merging ERA5-Land and IMERG precipitation (EIMD) can balance spatial-temporal patterns of precipitation and yields the most reliable precipitation estimates.

## 5. Conclusions

Large differences in precipitation products are the main uncertainties for water balance evaluation in the QTP. Our successful application of water balance and drought chain (WBDC) principles reveals that it is appropriate in areas that lack ground-based observations. The correlation between EDI based on diverse precipitation products and SMAP-based soil moisture anomaly as well as MODIS-based NDVI anomaly can predict the correlation between gauge observations and precipitation products with more confidence ($R = 0.785$). The water balance principle can distinguish precipitation climatology within watershed cells of diverse precipitation products. The simple average method for merging ERA5-Land and IMERG precipitation (EIMD), as proposed in this study, successfully reduces biases and verifies the water balance in both main basins and sub-basins while also clarifying the vegetation drought disaster chain in three herbaceous species areas in the Qinghai–Tibetan Plateau. Our proposed "down to top" surrounding assessment methodology enabled the assessment of precipitation datasets generated by remote sensing technology over a region with sparse observations. Drylands cover about 41% of Earth's land surface [66]. This emphasizes the potential of the "precipitation–soil–vegetation"

internal relationship perspective for water resource management in such remote or topographically complex areas.

**Author Contributions:** Methodology, R.L. and J.S.; software, R.L. and J.P.; investigation, R.L., T.Z., Q.Z. and Y.W.; writing—original draft preparation, R.L.; writing—review and editing, R.L., J.P. and N.Y. All authors have read and agreed to the published version of the manuscript.

**Funding:** This work has been jointly supported by the Second Tibetan Plateau Scientific Expedition and Research Program (STEP) (2019QZKK0206) and the National Natural Science Foundation of China (42071404, 41901271).

**Data Availability Statement:** The MODIS NDVI and SMAP remote sensing datasets used in this paper are all public datasets.

**Acknowledgments:** All authors would like to thank the editors and reviewers for their detailed comments and suggestions.

**Conflicts of Interest:** The authors declare no conflicts of interest.

## References

1. Yao, T.; Bolch, T.; Chen, D.; Gao, J.; Immerzeel, W.W.; Piao, S.; Su, F.; Thompson, L.G.; Wada, Y.; Wang, L.; et al. The imbalance of the Asian water tower. *Nat. Rev. Earth Environ.* **2022**, *3*, 618–632. [CrossRef]
2. Shiyi, L. The contemporary glaciers in China based on the second Chinese glacier inventor. *Acta Geogr. Sin.* **2015**, *70*, 3–16.
3. Zhan, C.; Chen, Y.; Yang, K.; La, Z.; Zhou, X.; Jiang, Y.; Ling, X.; Tian, J.; Wang, Y.; Li, X.; et al. First evaluation of GPM-era satellite precipitation products with new observations on the western Tibetan plateau. *Atmos. Res.* **2023**, *283*, 106559. [CrossRef]
4. Liu, J. Study on Spatial and Temporal Variation of the Boundary and Area of the Semi-Arid Region in Northern China over the Past 60 Years. Master's Dissertation, Northwest University, Xi'an, China, 2019.
5. Tong, K.; Su, F.; Yang, D.; Hao, Z. Evaluation of satellite precipitation retrievals and their potential utilities in hydrologic modeling over the Tibetan Plateau. *J. Hydrol.* **2014**, *519*, 423–437. [CrossRef]
6. Sun, Q.; Miao, C.; Duan, Q.; Ashouri, H.; Sorooshian, S.; Hsu, K. A Review of Global Precipitation Data Sets: Data Sources, Estimation, and Intercomparisons. *Rev. Geophys.* **2018**, *56*, 107–179. [CrossRef]
7. Lanza, L.G.; Stagi, L. Certified accuracy of rainfall data as a standard requirement in scientific investigations. *Adv. Geosci.* **2008**, *16*, 43–48. [CrossRef]
8. Brunetti, M.; Maugeri, M.; Monti, F.; Nanni, T. Temperature and precipitation variability in Italy in the last two centuries from homogenised instrumental time series. *Int. J. Climatol.* **2006**, *26*, 345–381. [CrossRef]
9. Herrera, S.; Kotlarski, S.; Soares, P.M.M.; Cardoso, R.M.; Jaczewski, A.; Gutiérrez, J.M.; Maraun, D. Uncertainty in gridded precipitation products: Influence of station density, interpolation method and grid resolution. *Int. J. Climatol.* **2019**, *39*, 3717–3729. [CrossRef]
10. Merino, A.; García-Ortega, E.; Navarro, A.; Fernández-González, S.; Tapiador, F.J.; Sánchez, J.L. Evaluation of gridded rain-gauge-based precipitation datasets: Impact of station density, spatial resolution, altitude gradient and climate. *Int. J. Climatol.* **2021**, *41*, 3027–3043. [CrossRef]
11. Yang, K.; Chen, Y.; Zhan, C.; Ling, X.; Zhou, X.; Jiang, Y.; Yao, X.; Lu, H.; Ma, X.; Ouyang, L.; et al. Cross-sectional rainfall observation on the central-western Tibetan plateau in the warm season: System design and preliminary results. *Sci. China Earth Sci.* **2023**, *66*, 1015–1030. [CrossRef]
12. Marek, R. Der Wasserhaushalt im Murgebiete. (Ein Beitrag zur Hydrographie der Mur). *Mitteilungen Des Naturwissenschaftlichen Ver. Für Steiermark* **1901**, *37*, 3–57. Available online: https://www.zobodat.at/pdf/MittNatVerSt_37_0003-0057.pdf (accessed on 21 December 2023).
13. Kirchner, J.W. Catchments as simple dynamical systems: Catchment characterization, rainfall-runoff modeling, and doing hydrology backward. *Water Resour. Res.* **2009**, *45*, W02429. [CrossRef]
14. Álvarez-Garretón, C.; Beck, H.E.; Wood, E.F.; McVicar, T.R.; Zambrano-Bigiarini, M.; Baez-Villanueva, O.M.; Sheffield, J.; Karger, D.N. Bias correction of global high-resolution precipitation climatologies using streamflow observations from 9372 catchments. *J. Clim.* **2019**, *33*, 1299–1315.
15. Yao, N.; Li, Y.; Lei, T.; Peng, L. Drought evolution, severity and trends in mainland China over 1961–2013. *Sci. Total Environ.* **2018**, *616–617*, 73–89. [CrossRef] [PubMed]
16. Zhu, Y.; Zhang, H.; Ding, M.; Li, L.; Zhang, Y. The multiple perspective response of vegetation to drought on the Qinghai Tibetan plateau. *Remote Sens.* **2023**, *15*, 902. [CrossRef]
17. Wu, W.; Li, Y.; Luo, X.; Zhang, Y.; Ji, X.; Li, X. Performance evaluation of the CHIRPS precipitation dataset and its utility in drought monitoring over Yunnan Province, China. *Geomat. Nat. Hazards Risk* **2019**, *10*, 2145–2162. [CrossRef]
18. Yu, L.; Leng, G.; Python, A. A comprehensive validation for GPM IMERG precipitation products to detect extremes and drought over mainland China. *Weather Clim. Extrem.* **2022**, *36*, 100458. [CrossRef]

19. Bai, X.; Shen, W.; Wu, X.; Wang, P. Applicability of long-term satellite-based precipitation products for drought indices considering global warming. *Environ. Manag.* **2019**, *255*, 109846. [CrossRef]
20. Sharma, S.; Khadka, N.; Hamal, K.; Shrestha, D.; Talchabhadel, R.; Chen, Y. How Accurately Can Satellite Products (TMPA and IMERG) Detect Precipitation Patterns, Extremities, and Drought Across the Nepalese Himalaya? *Earth Space Sci.* **2020**, *7*, e2020EA001315. [CrossRef]
21. Wilhite, D.A.; Glantz, M.H. Understanding: The drought phenomenon: The role of definitions. *Water Int.* **1985**, *10*, 111–120. [CrossRef]
22. Li, R.; Tsunekawa, A.; Tsubo, M. Index-based assessment of agricultural drought in a semi-arid region of inner Mongolia, China. *J. Arid Land* **2014**, *6*, 3–15. [CrossRef]
23. Hu, F.M.; Wei, Z.S.; Yang, X.N.; Xie, W.J.; Li, Y.X.; Cui, C.L.; Yang, B.B.; Tao, C.X.; Zhang, W.; Meng, L.K. Assessment of SMAP and SMOS soil moisture products using triple collocation method over Inner Mongolia. *J. Hydrol. Reg. Stud.* **2022**, *40*, 101027. [CrossRef]
24. Kogan, F.N. Global drought and flood-watch from NOAA polar-orbiting satellites. *Adv. Space Res.* **1998**, *21*, 477–480. [CrossRef]
25. Zheng, H.; Yang, Z.L.; Lin, P.; Wei, J.; Wu, W.Y.; Li, L.; Zhao, L.; Wang, S. On the Sensitivity of the Precipitation Partitioning Into Evapotranspiration and Runoff in Land Surface Parameterizations. *Water Resour. Res.* **2019**, *55*, 111–195. [CrossRef]
26. Akbar, R.; Gianotti, D.J.S.; Salvucci, G.D.; Entekhabi, D. Partitioning of Historical Precipitation Into Evaporation and Runoff Based on Hydrologic Dynamics Identified with Recent SMAP Satellite Measurements. *Water Resour. Res.* **2020**, *56*, e2020WR027307. [CrossRef]
27. Hare, F.K. Drought and desiccation-Twin hazards of a variable climate. In *Planning for Drought*; Whilhite, D., Easterling, W., Wood, D., Eds.; Westview Press: Boulder, CO, USA, 1987; pp. 3–9.
28. Georg, M.; Sabine, K.; Kaiser, J.; Liu, X.; Zhao, X. Status and Dynamics of the Kobresia Pygmaea Ecosystem on the Tibetan Plateau. *Ambio* **2008**, *37*, 272–279.
29. Pen-Chao, K.; Sun, Y.H. A preliminary study on the classification, distribution and ecological nature of genus *Stipa* L. of China. *Acta Phytotaxon. Sin.* **1982**, *20*, 34–44.
30. Lu, S.L.; Wu, Z.L. On Geographical Distribution of the Genus *Stipa* L. in China. *Acta Phytotaxon. Sin.* **1996**, *34*, 242–253.
31. Muñoz Sabater, J.; Dutra, E.; Agustí-Panareda, A.; Albergel, C.; Arduini, G.; Balsamo, G.; Boussetta, S.; Choulga, M.; Harrigan, S.; Hersbach, H.; et al. ERA5-land: A state-of-the-art global reanalysis dataset for land applications. *Earth Syst. Sci. Data* **2021**, *13*, 4349–4383. [CrossRef]
32. Huffman, G.J.; Bolvin, D.T.; Nelkin, E.J.; Tan, J. Integrated Multi-Satellite Retrievals for GPM (IMERG) technical documentation. *NASA Technol. Doc.* **2019**, *612*, 1–77. Available online: https://pmm.nasa.gov/sites/default/files/document_files/IMERG_doc_190909.pdf (accessed on 21 December 2023).
33. He, J.; Yang, K.; Tang, W.; Lu, H.; Qin, J.; Chen, Y.; Li, X. The first high-resolution meteorological forcing dataset for land process studies over China. *Sci. Data* **2020**, *7*, 25. [CrossRef] [PubMed]
34. Hong, Y.; Hsu, K.-L.; Sorooshian, S.; Gao, X. Precipitation estimation from remotely sensed imagery using an artificial neural network cloud classification system. *J. Appl. Meteor.* **2004**, *43*, 1834–1853. [CrossRef]
35. Jiang, Y.; Yang, K.; Shao, C.; Zhou, X.; Zhao, L.; Chen, Y.; Wu, H. A downscaling approach for constructing high-resolution precipitation dataset over the Tibetan Plateau from ERA5 reanalysis. *Atmos. Res.* **2021**, *256*, 105574. [CrossRef]
36. Beck, H.E.; Wood, E.F.; Pan, M.; Fisher, C.K.; Miralles, D.M.; van Dijk, A.I.J.M.; McVicar, T.R.; Adler, R.F. MSWEP V2 global 3-hourly 0.1° precipitation: Methodology and quantitative assessment. *Bull. Am. Meteorol. Soc.* **2019**, *100*, 473–500. [CrossRef]
37. Funk, C.; Peterson, P.; Landsfeld, M.; Pedreros, D.H.; Verdin, J.P.; Shukla, S.; Husak, G.; Rowland, J.; Harrison, L.; Hoell, A.; et al. The climate hazards infrared precipitation with stations—A new environmental record for monitoring extremes. *Sci. Data* **2015**, *2*, 150066. [CrossRef] [PubMed]
38. Xie, P.; Joyce, R.; Wu, S.; Yoo, S.; Yarosh, Y.; Sun, F.; Lin, R. Reprocessed, bias-corrected CMORPH global high-resolution precipitation estimates from 1998. *J. Hydrometeorol.* **2017**, *18*, 1617–1641. [CrossRef]
39. Zheng, C.L.; Jia, L.; Hu, G.C. Global land surface evapotranspiration monitoring by ETMonitor model driven by multi-source satellite earth observations. *J. Hydrol.* **2022**, *613*, 128444. [CrossRef]
40. Han, X.; Wu, J.; Zhou, H.; Liu, L.; Yang, J.; Shen, Q.; Wu, J. Intensification of Historical Drought over China Based on a Multi-model Drought Index. *Int. J. Climatol.* **2020**, *40*, 5407–5419. [CrossRef]
41. Rodell, M.; Houser, P.R.; Jambor, U.; Gottschalck, J.; Mitchell, K.E.; Meng, C.; Arsenault, K.R.; Cosgrove, B.; Radakovich, J.D.; Bosilovich, M.G.; et al. The Global Land Data Assimilation System. *Bull. Am. Meteorol. Soc.* **2004**, *85*, 381–394. [CrossRef]
42. Bai, P.; Liu, X. Intercomparison and evaluation of three global high-resolution evapotranspiration products across China. *J. Hydrol.* **2018**, *566*, 743–755. [CrossRef]
43. Byun, H.-R.; Wilhite, D.A. Objective quantification of drought severity and duration. *J. Clim.* **1999**, *12*, 2747–2756. [CrossRef]
44. Yong, B.; Wang, C.; Chen, J.; Chen, J.; Wang, T.; Li, L.; Barry, D.A. Missing water from the Qiangtang Basin on the Tibetan Plateau. *Geology* **2020**, *49*, 867–872. [CrossRef]
45. Tang, Q.; Lan, C.; Su, F.; Liu, X.; Sun, H.; Ding, J.; Wang, L.; Leng, G.; Zhang, Y.; Sang, Y.; et al. Streamflow change on the Qinghai-Tibet Plateau and its impacts. *Chin. Sci. Bull.* **2019**, *64*, 2807–2821.
46. Weligamage, H.G.; Fowler, K.; Tim, J.P.; Saft, M.; Murray, C.P.; Ryu, D. Partitioning of Precipitation into Terrestrial Water Balance Components under a Drying Climate. *Water Resour. Res.* **2023**, *59*, e2022WR033538. [CrossRef]

47. Lei, Y.; Li, R.; Husi, L.; Shi, J. Seasonal variations of recharge-storage-runoff process over the Tibetan Plateau. *J. Hydrometeorol.* **2023**, *24*, 1619–1633. [CrossRef]
48. Camici, S.; Christian, M.; Luca, C.; Ivan, M.; Luca, L.B. Which rainfall score is more informative about the performance in river discharge simulation? A comprehensive assessment on 1318 basins over Europe. *Hydrol. Earth Syst. Sci.* **2020**, *24*, 4869–4885. [CrossRef]
49. Liu, J.; Chai, L.; Lu, Z.; Liu, S.; Qu, Y.; Geng, D.; Song, Y.; Guan, Y.; Guo, Z.; Wang, J.; et al. Evaluation of SMAP, SMOS-IC, FY3B, JAXA, and LPRM Soil Moisture Products over the Qinghai-Tibet Plateau and Its Surrounding Areas. *Remote Sens.* **2019**, *11*, 792. [CrossRef]
50. Zhang, Y.; Huang, Y.; Xu, H.; Wang, S.; Long, T.; Zhao, Q. Evaluation of Precipitation Frequency and Intensity as Estimated by the GPM IMERG Precipitation Product at Daily and Hourly Scales over the Tibetan Plateau. *Atmosphere* **2023**, *14*, 1653. [CrossRef]
51. Aksu, H.; Taflan, G.Y.; Yaldiz, S.G.; Akgl, M.A. Evaluation of IMERG for GPM satellite-based precipitation products for extreme precipitation indices over Turkiye. *Atmos. Res.* **2023**, *291*, 106826. [CrossRef]
52. Li, R.; Wang, J.; Zhao, T.; Shi, J. Index-based Evaluation of Vegetation Response to Meteorological Drought in Northern China. *Nat. Hazard* **2016**, *84*, 2179–2193. [CrossRef]
53. Liu, Y.; Wu, C.; Jassal, R.S.; Wang, X.; Shang, R. Satellite Observed Land Surface Greening in Summer Controlled by the Precipitation Frequency Rather Than Its Total Over Tibetan Plateau. *Earths Future* **2022**, *10*, e2022EF002760. [CrossRef]
54. Serrano, S.M.; Gouveia, C.M.; Camarero, J.J.; Beguería, S.; Trigo, R.M.; López-Moreno, J.I.; Azorín-Molina, C.; Pasho, E.; Lorenzo-Lacruz, J.; Revuelto, J.; et al. Drought Impacts on Vegetation Activity, Growth and Primary Production in Humid and Arid Ecosystems. In Cambio Climático. Extremos e Impactos: Ponencias Presentadas al VIII Congreso Internacional de la Asociación Española de Climatología, Asociación Española de Climatología. 2012, pp. 691–699. Available online: https://digital.csic.es/bitstream/10261/126669/1/44-Extremos.pdf (accessed on 21 December 2023).
55. Wang, P.; Huang, K.; Hu, S. Distinct fine-root responses to precipitation changes in herbaceous and woody plants: A meta-analysis. *New Phytol.* **2020**, *225*, 1491–1499. [CrossRef] [PubMed]
56. Zhang, G.; Chen, W.; Xie, H. Tibetan Plateau's lake level and volume changes from NASA's ICESat/ICESat-2 and Landsat Missions. *Geophys. Res. Lett.* **2019**, *46*, 13107–13118. [CrossRef]
57. Kaya, Y.; Sanli, F.B.; Abdikan, S. Determination of long-term volume change in lakes by integration of UAV and satellite data: The case of Lake Burdur in Türkiye. *Environ. Sci. Pollut. Res. Int.* **2023**, *30*, 117729–117747. [CrossRef] [PubMed]
58. Ghorbanian, A.; Mohammadzadeh, A.; Jamali, S.; Duan, Z. Performance Evaluation of Six Gridded Precipitation Products throughout Iran Using Ground Observations over the Last Two Decades (2000–2020). *Remote Sens.* **2022**, *14*, 3783. [CrossRef]
59. Bai, L.; Wen, Y.; Shi, C.; Yang, Y.; Zhang, F.; Wu, J.; Gu, J.; Pan, Y.; Sun, S.; Meng, J. Which Precipitation Product Works Best in the Qinghai-Tibet Plateau, Multi-Source Blended Data, Global/Regional Reanalysis Data, or Satellite Retrieved Precipitation Data? *Remote. Sens.* **2020**, *12*, 683. [CrossRef]
60. Anjum, M.N.; Irfan, M.; Waseem, M.; Leta, M.K.; Niazi, U.M.; Rahman, S.; Ghanim, A.A.; Mukhtar, M.A.; Nadeem, M.U. Assessment of PERSIANN-CCS, PERSIANN-CDR, SM2RAIN-ASCAT, and CHIRPS-2.0 rainfall products over a semi-arid subtropical climatic region. *Water* **2022**, *14*, 147. [CrossRef]
61. Zambrano-Bigiarini, M.; Nauditt, A.; Birkel, C.; Verbist, K.; Ribbe, L. Temporal and spatial evaluation of satellite-based rainfall estimates across the complex topographical and climatic gradients of Chile. *Hydrol. Earth Syst. Sci.* **2016**, *21*, 1295–1320. [CrossRef]
62. Ali, S.; Chen, Y.; Azmat, M.; Kayumba, P.M.; Ahmed, Z.; Mind'je, R.; Ghaffar, A.; Qin, J.; Tariq, A. Long-term performance evaluation of the latest multi-source weighted-ensemble precipitation (MSWEP) over the highlands of indo-pak (1981–2009). *Remote. Sens.* **2022**, *14*, 4773. [CrossRef]
63. Adam, J.C.; Lettenmaier, D.P. Adjustment of global gridded precipitation for systematic bias. *J. Geophys. Res.* **2003**, *108*, 4257. [CrossRef]
64. Wu, X.; Su, J.; Ren, W.; Lü, H.; Yuan, F. Statistical comparison and hydrological utility evaluation of ERA5-Land and IMERG precipitation products on the Tibetan Plateau. *J. Hydrol. Part A* **2023**, *620*, 129384. [CrossRef]
65. Tang, G.; Clark, M.P.; Papalexiou, S.M.; Ma, Z.; Hong, Y. Have satellite precipitation products improved over last two decades? A comprehensive comparison of GPM IMERG with nine satellite and reanalysis datasets. *Remote Sens. Environ.* **2020**, *240*, 111697. [CrossRef]
66. Food and Agriculture Organization (FAO). *Trees, Forests and Land Use in Drylands: The First Global Assessment–Full Report*; FAO Forestry Paper; FAO: Rome, Italy, 2019; Volume 184, Available online: https://reliefweb.int/attachments/b109dfbf-734c-3928-a375-2c87de0d76f8/CA7148EN.pdf (accessed on 21 December 2023).